DYNA
ISSN: 0012-7353
ISSN: 2346-2183
Universidad Nacional de Colombia

Cardenas-Flechas, Leydi Julieta; Raba, Angela Mercedes; Rincón-Joya, Miryam
Synthesis and evaluation of nickel doped Co3O4 produced through hydrothermal technique
DYNA, vol. 87, no. 213, 2020, April-June, pp. 184-191
Universidad Nacional de Colombia

DOI: https://doi.org/10.15446/dyna.v87n213.84410

UNIVERSIDAD
NACIONAL
DE COLOMBIA
SEDE MEDELLÍN
FACULTAD DE MINAS

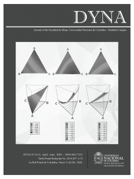

DYNA
http://dyna.medellin.unal.edu.co/

Synthesis and evaluation of nickel doped Co_3O_4 produced through hydrothermal technique

Leydi Julieta Cardenas-Flechas [a] Angela Mercedes Raba [b] & Miryam Rincón-Joya [c]

[a] *Departamento de Ingeniería Mecánica y Mecatrónica, Facultad de Ingeniería, Universidad Nacional de Colombia, Bogotá, Colombia. ljcardenasf@unal.edu.co*
[b] *Departamento de Física, Facultad de Ciencias, Universidad Francisco de Paula Santander, Cúcuta, Colombia. amrabap@gmail.com*
[c] *Departamento de Física, Facultad de Ciencias, Universidad Nacional de Colombia, Bogotá, Colombia. mrinconj@unal.edu.co*

Received: January 3rd, 2020. Received in revised form: April 3rd, 2020. Accepted: April 15th, 2020

Abstract
The synthesis of undoped cobalt oxide and cobalt oxide with 4%nickel doping is studied in samples obtained through hydrothermal technique. After the final heat treatment at 300°C, X-ray diffraction analysis indicated the formation of cobalt spinel oxide with a complete replacement of nickel in the lattice. An average crystallite size of ~42 nm and ~31nm was found, as well as a particle size of ~ 20 nm and ~30 nm for Co_3O_4 and $Co_{3-x}Ni_xO_4$, respectively. Structural parameters were established through Rietveld refinement with a good correspondence between the simulated and the experimental pattern with values of $x^2 = 1.25$ and GOF = 0.90 for Co_3O_4. The energy band gap was found through UV-Vis spectroscopy in two different regions: Eg_1 and Eg_2 values vary between 1.54 and 2.04eV for samples doped with nickel. The SEM results indicated the formation of nanostructures with semi-cubic shape and irregular rods. Parameters such as crystal size, particle size, surface area, as well as morphology of the final product depend on doping.

Keywords: cobalt oxide; doping, nanostructures; structural parameters.

Síntesis y evaluación de Co_3O_4 dopado con níquel producido mediante la técnica hidrotermal

Resumen
La síntesis de óxido de cobalto con dopaje de níquel al 4% se estudia en muestras obtenidas mediante técnica hidrotermal. Después del tratamiento térmico final a 300°C, el análisis de difracción de rayos X indicó la formación de óxido de cobalto espinela con una substitución completa de níquel en la red. Se encontró un tamaño promedio de cristalito de ~42 nm ~31 nm, así como un tamaño de partícula de ~20 nm y ~30 nm para Co_3O_4 y $Co_{3-x}Ni_xO_4$, respectivamente. Los parámetros estructurales se establecieron mediante refinamiento Rietveld con una buena correspondencia entre el patrón simulado y el experimental con valores de $X^2 = 1.25$ y GOF = 0.90 para Co_3O_4. La brecha de banda de energía se encontró a través de espectroscopía UV-Vis en dos regiones diferentes, los valores Eg_1 y Eg_2 varían entre 1.54 y 2.04eV para muestras dopadas con níquel. Los resultados SEM indicaron la formación de nanoestructuras con forma semicúbica y bastones irregulares. Parámetros tales como el tamaño del cristal, el tamaño de partícula, el área de superficie, así como la morfología del producto final dependen del dopaje.

Palabras clave: óxido de cobalto; dopaje; nanoestructuras; parámetros estructurales.

1. Introduction

Metal oxides such as iron, cobalt, copper and zinc are candidates for a variety of important technological applications in catalysis, solar energy conversion, electronics, magnetic media storage, etc. [1]. Recently, nanomaterials based on such oxides have been developed for various applications. Among these nanomaterials, Co3O4 cobalt oxide has several morphologies and advantages, such as biological compatibility, broadband, high stability and low

---

How to cite: Cardenas-Flechas, L.J, Raba, A.M. and Rincón-Joya, M, Synthesis and evaluation of nickel doped Co3O4 produced through hydrothermal technique. DYNA, 87(213), pp. 184-191, April - June, 2020.

Revista DYNA, 87(213), pp. 184-191, April - June, 2020, ISSN 0012-7353
DOI: http://doi.org/10.15446/dyna.v87n213.84410

cost [2]. Due to its good reproducibility and selectivity, this material has also been explored in fields such as supercapacitors and electrochemical sensors [3-5].

It is known that the behavior of nanophase materials depends largely on the shapes and sizes of the particles, which are, therefore, key factors in their performance and final applications [6]. Different electrical, optical, magnetic and mechanical properties in semiconductors can be achieved with a controlled size of nanoparticles. Nanostructured porous materials also have applications such as gas sensors, catalysis, among others [7,8]. Transition metal oxides with various oxidation states are very promising candidates for the high capacitance of the next generation, including nickel oxide. Regarding nickel, it has shown a very high specific capacity, low cost, low toxicity and respect for the environment, but with a relatively low cyclic reversibility [9].

The synthesis of cobalt oxide compounds with adjustable physicochemical properties has become a research point, where doping with transition metals improves properties such as electrical behavior as well as optical absorption [10]. Specifically, doping of Co_3O_4 with nickel has shown significant changes in the behavior of the material. Improvement in the catalytic activity for the oxidation of CO through hybrid matrices is found in the most recent works of nickel doped Co_3O_4 [11]. Wang et al. [9] evaluated the performance of solar-powered steam as a possible candidate for solar photothermal conversion using Co_3O_4 nanoforest / Ni foam. Li et al. [12] analyzed the ORR activity according to the influence of nickel doping content. Ouyang et al. [13] concluded the excellent capacitive performance of the composite material attributed to the improved charge transfer rate and ion diffusion path. Additionally, Ren et al. [14] indicated that doping with Ni in the spinel lattice of Co_3O_4 improves reaction kinetics and promotes catalytic activity.

In the present research, Co_3O_4 and Co_3O_4 doped with 4% nickel were synthesized by the hydrothermal technique and then calcining them at 300°C. The products obtained will be characterized using different techniques, such as X-ray diffraction and subsequently Rietveld refinement analysis. Samples of Co_3O_4 have a crystalline structure after final heat treatment, and secondary phases belonging to the precursors used in the synthesis. SEM was used to observe the particle size and band gap results were obtained by UV-Vis. The research seeks to establish a comparison between Co_3O_4 and $Co_{3-x}Ni_xO_4$ x=0.04 studying the effect of hydrothermal synthesis.

2. Materials and methodology

2.1. *Preparation of Co_3O_4*

The synthesis was performed following the procedure of Jin et al. [15]. Initially, cobalt acetate and distilled water were used in the synthesis, then, urea and ammonia were added with constant stirring. The solution was carried in an autoclave for 20 hours at a temperature of 180 ° C. Finally, the sample was washed with distilled water twice and the powders obtained were calcined at 300 ° C for 3h.

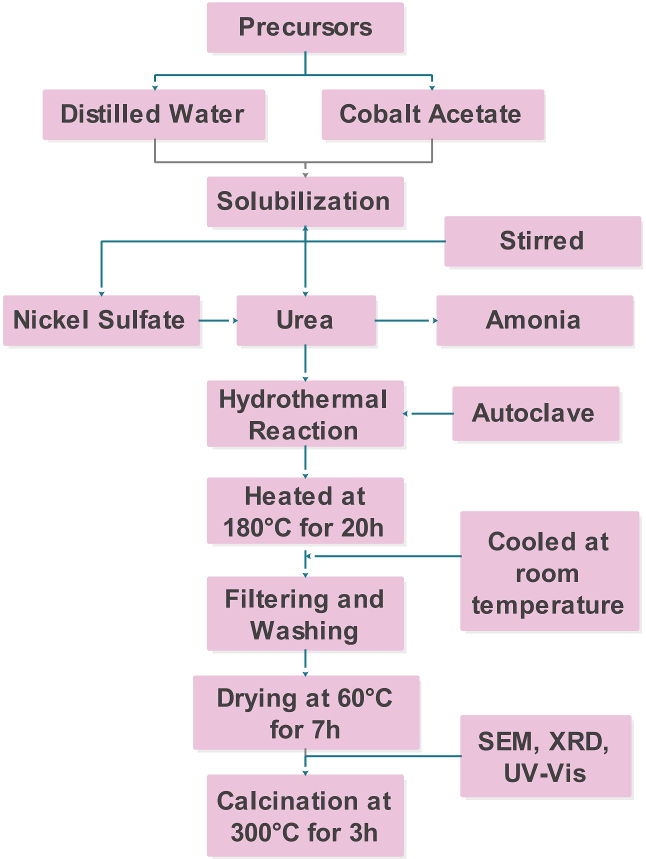

Figure 1. Schematic diagram of the hydrothermal process of Co_{3-x} Ni_xO_4 preparation.
Source: The Authors.

2.2. *Preparation Co_3O_4 / Ni (4%)*

Cobalt acetate was dissolved in distilled water. After solubilizing the components, nickel sulfate and, subsequently, urea were added. 2ml of ammonia were also added to adjust the pH. The solution was transferred to an autoclave and heated for 20 hours at 180°C. The samples obtained were washed with distilled water and ethanol and dried for 7 hours at 60°C. Finally, the powders were calcined at 300°C for 3 hours. Fig. 1 shows the schematic diagram of the hydrothermal process for the synthesis of nickel-doped Co_3O_4.

2.3. *Characterization*

The characterization of the samples was carried out using the techniques described below. The X-ray diffraction analysis (XRD) was performed on a PANalytical X'pert Pro equipment with data taken at an angle 2 between 100 and 800. It uses a RTMS (real time multiple strip) detector with CuKα radiation, a wavelength of $\lambda = 1.542Å$ and a step of 0.02630 in Brentano Bragg mode, with subsequent Rietveld refinement of the experimental data, using the GSAS II code.

A Cary5000 UV-Vis-NIR diffractometer was used for measuring the UV-Vis reflectance spectrum in diffuse reflectance mode in the 200-2500 nm wavelength range.

With the aim to study the optical response of the Co_3O_4, the samples were measured with UV-visible electronic absorption spectroscopy. The morphological analysis was performed with a FEI Quanta 200 scanning electron microscope (SEM), in secondary electron mode at high vacuum and voltage of 30 KV. The qualitative chemical composition analysis was performed via energy dispersion microscopy (EDS).

3. Results and discussion

3.1. *Structural characterization*

The spinel structure tolerates a high concentration of defects. This allows its physicochemical properties to be adjusted by doping and the insertion of several transition metals with various oxidation states at the spinel structure sites. The doping of Co_3O_4 with nickel improves the electrical conductivity, which is related to the occupation of the doping site and its state of valence [16]. Fig. 2 shows the substitution of nickel at sites $^{2+}$ and $^{3+}$ of Co_3O_4. When nickel is added, it substitutes preferably the octahedral sites of Co^{3+} through stabilization at sites $^{2+}$ and $^{3+}$ [17]. According to Koneru et al. [18], Ni^{2+} at the tetrahedral sites leads to a normal spinel, while Ni^{2+} at the octahedral sites leads to an inverse spinel or a partial inverse spinel structure.

Fig. 3 shows the X-ray diffraction (XRD) pattern of Co_3O_4 powder with the subsequent final heat treatment at 300°C for 3 hours and Co_3O_4 doped with Ni and calcined during the same time. In section (a), the precursors obtained by the hydrothermal technique and examined by XRD are crystalline, though it is difficult to assign the definitive pattern to a specific phase. This condition has been present in other deposits [13]. In section (b), Co_3O_4 was calcined at 300°C for 3h in air and the crystallinity of Co_3O_4 is observed. In section (c), the pattern corresponds to the synthesis of $Co_{3-x}Ni_xO_4$ x=0.04, where the precursor peaks are observed again. Finally, in section (d), the pattern corresponds to Co_{3-x} Ni_x O_4 x=0.04 after final heat treatment at 300°C-3h, where the intermediate peaks disappear completely and other diffraction peaks correspond to crystalline non-detected products. This indicates the high purity of the final heat treatment product.

All the powders obtained show diffraction peaks coinciding with the Co_3O_4 cubic spinel structure (space group *F-4 3m*) with file COD 00-001-1152. This agrees with other researches [13,19,20]. The XRD pattern with reflection peaks is associated with the planes (220), (311), (222), (400), (422), (511) and (440) at 2θ = 31.27°, 36.88°, 38.62°, 44.81°, 55.75°, 59.45° and 65.38°, respectively, and with the plane $\langle 311 \rangle$ as preferential orientation. The 2θ position peaks observed in (a) and (c) at 24.01°, 32.69°, 34.69° are associated with the precursors used in the synthesis as $(Co(C_2H_3O_2)_2{\cdot}4H_2O$ cobalt acetate. According to Singhal et al. [21], when the doping of nickel is carried out in Co_3O_4, a slight displacement is observed in the diffraction peaks.

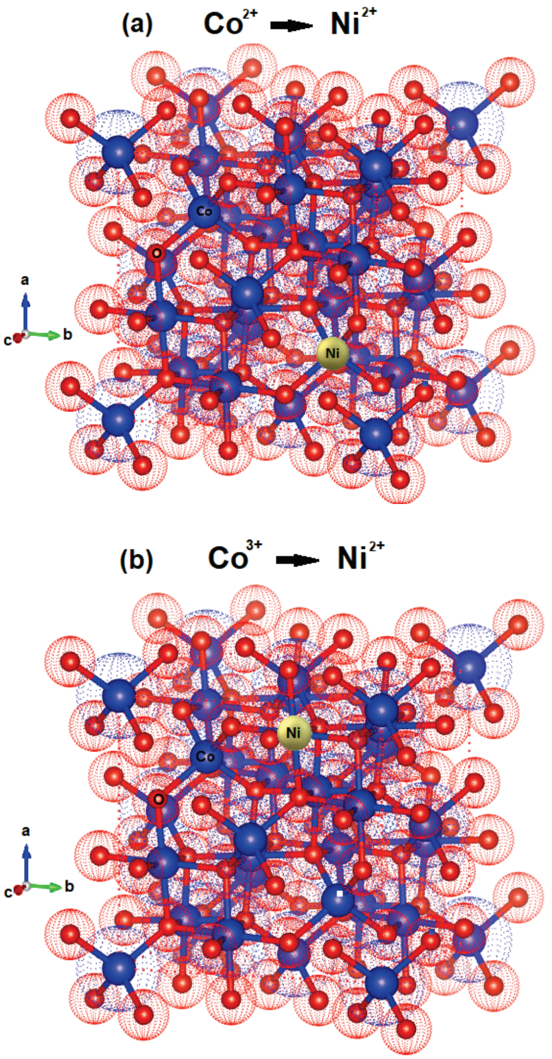

Figure 2. Bulk structure of spinel Co_3O_4 with single tetragonal Co^{2+} cations (a) and single octahedral Co^{3+} (b), being replaced by Ni^{2+} cations.
Source: The Authors using software Vesta.

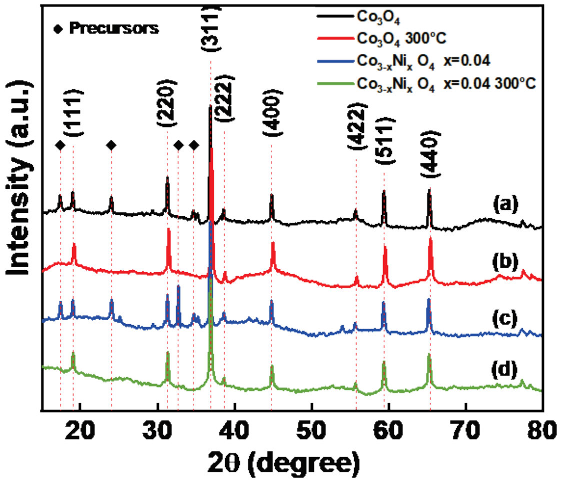

Figure 3. X-ray spectra (XRD) for the Co3O4 samples obtained via hydrothermal technique: (a) Co_3O_4, (b) Co_3O_4 300°C (c) Co_{3-x} Ni_xO_4 x=0.04 and (d) Co_{3-x} Ni_xO_4 x=0.04-300°C.
Source: The Authors.

Table 1.
Chemical composition of samples of Co_3O_4 doped with nickel

Co_3O_4		Co_3O_4-300°C		$Co_{3-x}Ni_xO_4$ x=0.04		$Co_{3-x}Ni_xO_4$ x=0.04 300°C	
El.	**% at**	**El.**	**% at**	**El.**	**% at**	**El.**	**% at**
Co K	8.07	Co K	28.39	Co K	6.34	Co K	27.91
O K	44.08	O K	55.30	O K	56.97	O K	46.07
C K	8.07	C K	16.31	C K	36.37	C K	24.59
				Ni K	0.32	Ni K	1.43

Source: The Authors.

Table 1 shows the energy-dispersive spectrometry (EDS) analysis with the percentages of atomic concentration. Results indicate the presence of elements of Co_3O_4 calcined at 300°C, as well as Co_3O_4 doped with nickel and calcined. Elements such as Co, O, C and Ni appear according to the synthesis of each of the compounds.

In order to establish structural parameters and properties, Rietveld refinement was carried out with the experimental data using the GSASII code. Fig.4 (a) corresponds to Co_3O_4 and Fig. 4 (b) to $Co_{3-x}Ni_xO_4$ x=0.04- 300°C. The quality of the refinement can be checked through the values of the main refinement parameters: x^2=1.25 and 1.26, R_{wp}= 0.89%, and 1.17% for $Co_{3-x}Ni_xO_4$ x=0.04-300°C. There is a good correspondence between the simulated and experimental pattern. Table 2 shows the lattice parameters of the refinement and in Table 3 the positions of Co_3O_4 are observed. The refinement allowed to determine that Co_3O_4 crystallizes in a spinel structure with a spatial group *F-43m* and with lattice parameters a=b=c=8.092630Å. The refinement parameters are shown in Table 4, where values of GOF 0.90 and 1.13 are observed for Co_3O_4 and $Co_{3-x}Ni_xO_4$ x=0.04-300°C, respectively. It has been observed that the lattice parameter and the unit cell volume for Co_3O_4 are close to those found in the literature [22-24]. According to Mulinari et al. [25] the variation in the observed atomic positions in the oxygen atoms may be associated with the formation of distortions in the bonds [O-Co-O].

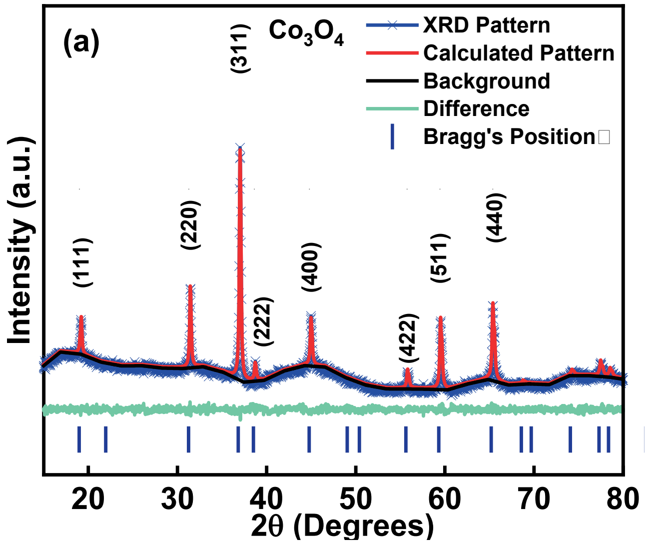

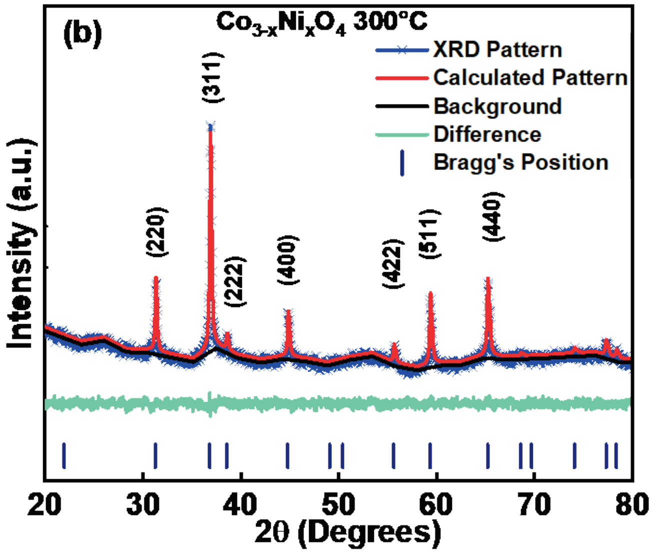

Figure. 4 XRD refined pattern for the Co_3O_4 -300°C. Blue symbols represent the experimental diffraction data. The continuous line is the calculated pattern and the difference between the experimental and calculated patterns is represented by the base line.
Source: The Authors.

Table 2.
Lattice parameters Co_3O_4

Co_3O_4 Lattice Refinement parameters					
a (Å)	**b (Å)**	**c (Å)**	**α**	**β**	**γ**
8.092630	8.092630	8.092630	90°C	90°C	90°C

Source: The Authors.

Table 3.
Positions Co_3O_4

Co_3O_4 Positions			
	x	**y**	**z**
Co1	0.0000	0.0000	0.0000
Co2	0.2500	0.2500	0.2500
Co3	0.6250	0.6250	0.6250
O1	0.3900	0.3900	0.3900
O2	-0.1400	-0.1400	-0.1400

Source: The Authors.

Table 4.
Refinement parameters.

Refinement parameters Co_3O_4						
x^2	**R_{esp}**	**R_E**	**R(BS)**	**R_{wp} (BS)**	**GOF**	**Vol(Å)**
1.25	1.00%	0.71%	0.96%	0.89%	0.90	529.992
Refinement parameters $Co_{3-x}Ni_xO_4$ x=0.04 - 300°C						
x^2	**R_{esp}**	**R_E**	**R(BS)**	**R_{wp} (BS)**	**GOF**	**Vol(Å)**
1.26	1.04%	0.99%	1.23%	1.17%	1.13	529.854

Source: The Authors.

3.2. Surface microstructure and composition

In Fig. 5, (a) and (c) indicate the SEM images of the precursors and (b) and (d) the products of Co_3O_4 after final heat treatment. In (a), there are particles with semicircular forms, most of them well defined. In (b), agglomerations appear with certain rods in some of the particles. In (c), the

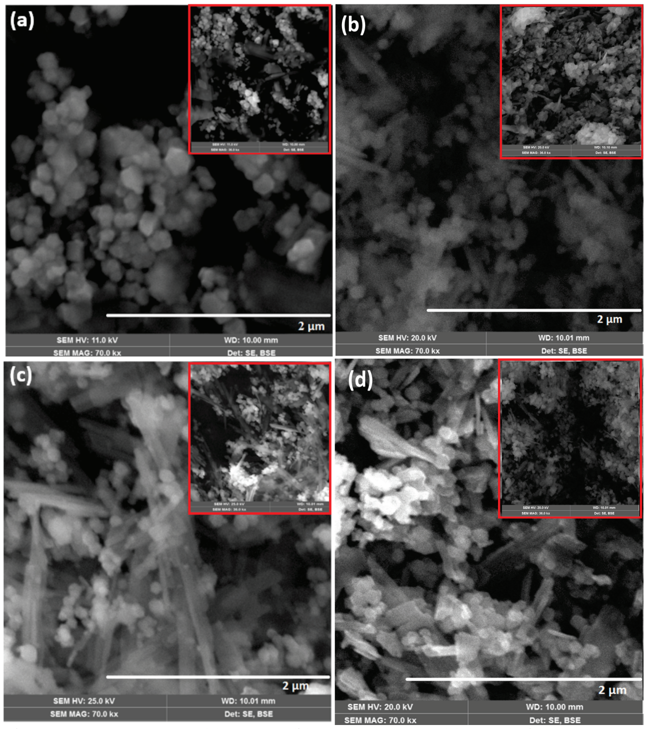

Figure. 5 SEM Images (a) Co_3O_4 (b) Co_3O_4 -300°C(c) $Co_{3-x}Ni_xO_4$ (d) $Co_{3-x}Ni_xO_4$ -300°C.
Source: The Authors.

rods are notorious due to their diameter, and there are several particles. In (d), the structure is rather rough and has no definite shape. Irregular shapes are appreciated with agglomerations and certain inclusions that are attributed to nickel. The different forms obtained at 300 ° in (b) and (d) at 300°C are associated with the addition of nickel in the dopage in (d). Depending on the concentration of reagents, Co_3O_4 nanoparticles with different shapes can be obtained [26].

It is assumed that temperature can affect surface morphology. According to Rajeshkhanna et al. [27], different sizes of anions embedded in the reaction mixture are responsible for the formation of different morphologies during the growth of the cobalt oxide material. The preferential adsorption/desorption of anions in specific crystallographic planes controls the formation of different morphologies, as well as the decrease in their surface energy.

Fig. 6 shows the process for synthesizing nickel-doped cobalt oxide. Initially, the mixture of nickel and cobalt is constantly stirred, with subsequent heating in the autoclave. Then, it was washed and dried.

As a result, nanostructures with semicubic and irregular rods were obtained. The autoclave was heated at 180°C for 20h (3°C/min), drying was carried out for 7h at 60 ° C in an oven, and the powders obtained were finally calcined in air at 300°C for 3h (10°C/min).

Organic and inorganic additives can be used to allow the precise control of various reaction parameters in the resulting composition, shape and size of nanocrystals, thanks to the liquid phase synthesis [28-30].

The average particle sizes were calculated by using the Debye Scherrer equation (0.9λ / (βcosθ)) and obtaining the average crystallite size. The term λ is the wavelength, from full width to maximum half (FWHM) of the diffraction peak, and θ is the Bragg Angle. The average particle size was calculated by using the most intense peak (<hkl>), (311). The crystallite size for Co_3O_4 and $Co_{3-x}Ni_xO_4$ x=0.04 was found at an average of 41.575nm with a slight decrease when nickel is added. For Co_3O_4 at 300° C, the crystallite size decreases approximately 8 nm compared with Co_3O_4 without final heat treatment and with a value of 33.85nm, and $Co_{3-x}Ni_xO_4$ x=0.04 300°C at 12nm with a value of 29.89nm, as shown in Table 5. These results agree with the works of Singhal et al. [21,31] where the peaks represent a good crystallinity and they obtained a crystallite size of 36-42nm.

Table 5.
Crystallite size calculation using the Debye Scherrer equation

Sample	Peak position (2θ)	FWHM (degree)	Crystallite size (nm)
Co_3O_4	36.85	0.1991	42.04
Co_3O_4 300°C	37.03	0.2474	33,85
Co_{3-x} Ni_x O_4 x=0.04	36.87	0.2036	41.11
Co_{3-x} Ni_x O_4 x=0.04 300°C	36.91	0.2801	29.89

Source: The Authors.

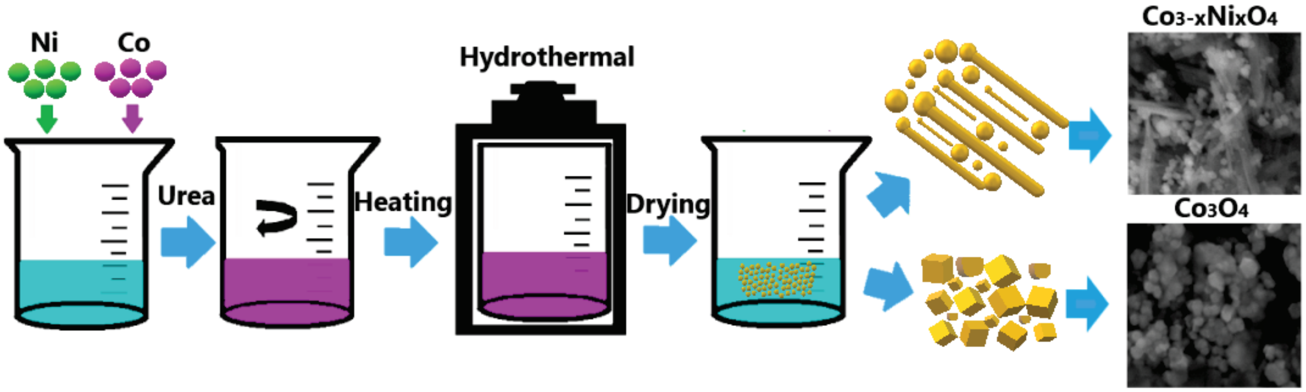

Figure. 6 Schematic illustration of the fabrication process of Co_3O_4 - $Co_{3-x}Ni_xO_4$.
Source: The Authors.

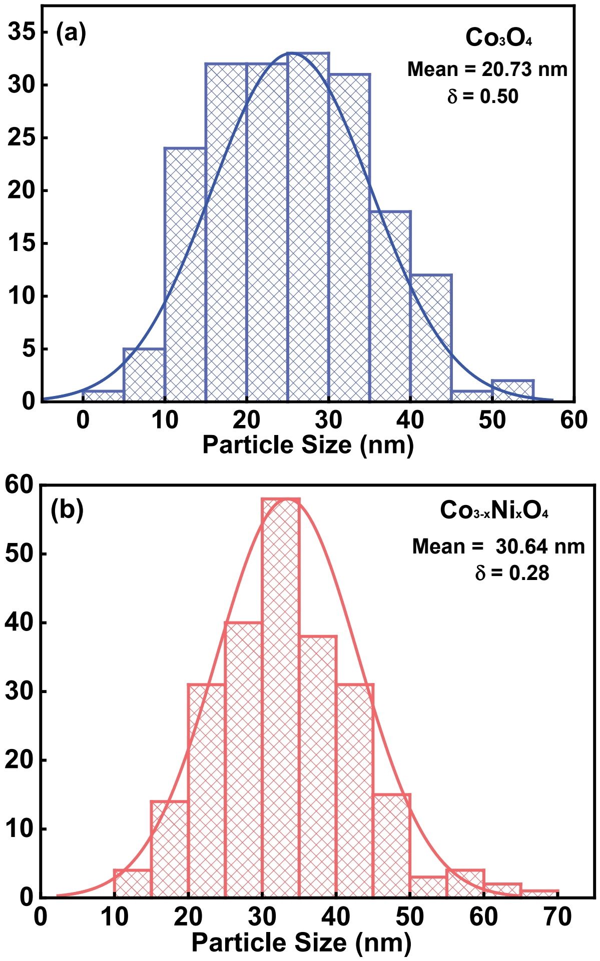

Figure 7. Particle Size: (a) Co_3O_4 and (b) Co_{3-x} Ni_xO_4 x=0.04
Source: The Authors.

These results can also be associated with the research by Lakehal et al. [10], who prepared films and fine powders of nickel-doped cobalt oxide on glass substrates. They used an immersion coating process based on sol gel with a concentration of Ni in the range from 0 to 9% by weight (%). The crystallite size of the samples was in the range of 214-279 Å. According to Itteboina et al. [32], the heat treatment has an important role in particle size. Additionally, the crystallite size may be directly related to the nucleation table [33].

Fig. 7 shows the particle diameter size for (a) Co_3O_4 that corresponds to 20.73nm and (b) Co_{3-x} Ni_xO_4 of 30.64nm. This size increases when cobalt oxide is doped with nickel. The difference is approximately 9.91 nm. It has been found that nickel substitution improves cobalt-spinel oxide activity by enlarging its specific surface area, its conductivity and its roughness factor, which is also called electronic and geometric effect [34].

3.3. *Optical band gap determination*

Fig. 8 (a) shows the UV-Vis diffuse reflectance spectra of Co_3O_4 alone and doped with 4% nickel, both calcined at 300°C. In the spectrum, the bandwidth values were calculated for the four samples shown in Table 6. The Eg_1 value found is Eg_1 = 1.51eV and correspond to $O^{-2} \rightarrow Co^{3+}$ [35], while for Eg_2, the value is Eg_2 = 2.74eV. For the Co_3O_4 doped with 4% Ni, there is a slight increase in the band gap compared with pure Co_3O_4. The gap energy changed from 1.51eV for pure Co_3O_4 to 1.55eV for the Co_3O_4 doped with 4% Ni. For the calcined Co_3O_4 doped with 4% Ni, there was also an increase compared with Co_3O_4 at 300 ° C (1.53eV for Co_3O_4 at 300°C and 1.56eV for Co_3O_4 at 300 ° C with 4% Ni). The highest bandwidth energy changed from 2.74eV for Co_3O_4 to 1.54eV for Co_3O_4 at 300°C. This behavior can be attributed to the lattice distortions caused by the temperature change, as well as to the introduction of nickel ions in the Co_3O_4 matrix and the formation of impurity energy levels (acceptor level) [10]. The morphology and structures of the materials are closely related to their optical properties, which are more evident in nanomaterials [36].

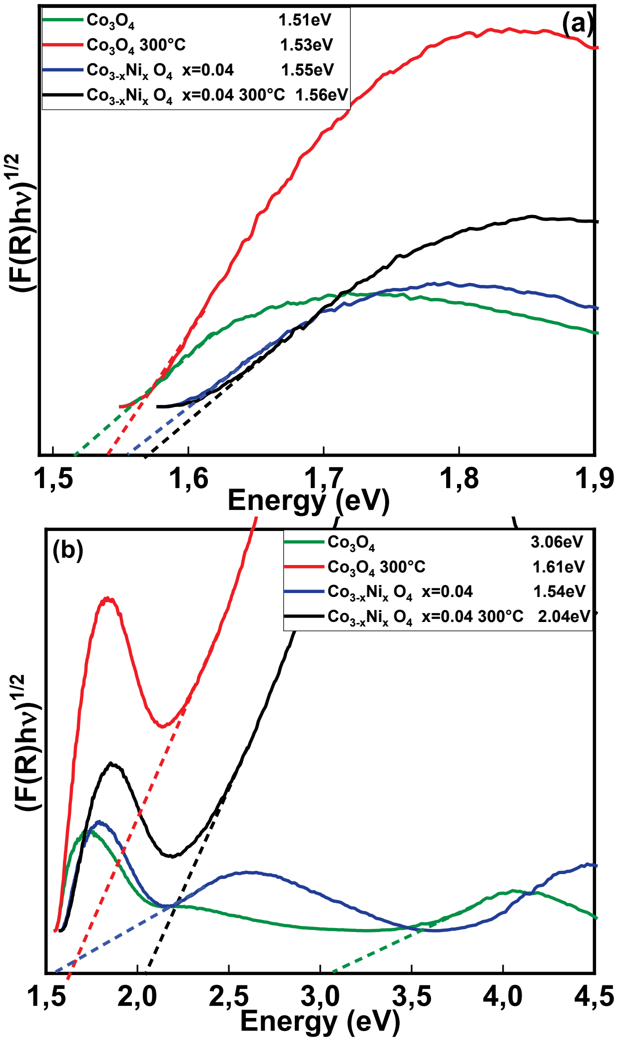

Figure 8. Determination of the band interval for Co_3O_4, Co_3O_4 at 300°C, Co_{3-x} Ni_xO_4 x=0.04 and Co_{3-x} Ni_xO_4 x=0.04 at 300°C for (a) the first region and (b) the second region.
Source: The Authors.

Table 6.
Band Gap values for the first and second regions

Sample	Eg_1(eV)	Eg_2(eV)
Co_3O_4	1.51	2.74
Co_3O_4 300°C	1.53	1.61
$Co_{3-x}Ni_xO_4$ x=0.04	1.55	1.54
$Co_{3-x}Ni_xO_4$ x=0.04 300°C	1.56	2.04

Source: The Authors.

4. Conclusions

Compounds of Co_3O_4 and Co_{3-x} Ni_xO_4 with nickel doping were synthesized and the subsequent final heat treatment was performed at 300°C through the hydrothermal technique. After heat treatment, the results obtained indicated the crystallinity of Co_3O_4 without the presence of Ni or NiO_x impurities, according to the X-ray diffraction analysis. In the Co_{3-x} Ni_xO_4 compound, the heat treatment at 300°C allowed the conversion of the precursor to particles.

Structural characterization in samples of Co_3O_4 and Co_{3-x} Ni_xO_4 was found through Rietveld refinement of experimental X-ray diffraction data. This evidenced that the samples initiate its major crystallization into a cubic structure belonging to the spatial group *F-43m* (# 216) with cell parameters a=b=c= 8.092630 Å with a slight variation in the volume value of the unit cell and a lower value for the nickel-doped compound of 529.584Å. The particle size varies between 20 and 30nm. Optical band gap measurements allowed to establish the value of Eg_1 and Eg_2 between 1.51 and 2.74eV for the samples of Co_3O_4 calcinated and with doping.

References

[1] Mehmood, S,. Synthesis and characterizations of Co_3O_4 based nanocomposite for electrochemical sensor applications. PhD Thesis, Faculty of Science, Malasya University, Malasya, 2018.

[2] Ding, L., Zhao, M., Fan, S., Ma, Y., Liang, J., Wang, X. and Chen, S., Preparing Co_3O_4 urchin-like hollow microspheres self-supporting architecture for improved glucose biosensing performance. Sensors and Actuators, B: Chemical, 235, pp. 162-169, 2016. DOI: 10.1016/j.snb.2016.05.068.

[3] Hoa, L.T., Chung, J.S. and Hur, S.H., A highly sensitive enzyme-free glucose sensor based on Co_3O_4 nanoflowers and 3D graphene oxide hydrogel fabricated via hydrothermal synthesis. Sensors and Actuators, B: Chemical, 223, pp. 76-82, 2016. DOI: 10.1016/j.snb.2015.09.009.

[4] Dalkiran, B., Kaçar, C., Erden, P.E., and Kiliç, E., Amperometric xanthine biosensors based on chitosan- Co_3O_4- multiwall carbon nanotube modified glassy carbon electrode. Sensors and Actuators, B: Chemical, 2014, pp. 83-91, 2014. DOI: 10.1016/j.snb.2014.04.025.

[5] Qing, X., Liu, S., Huang, K., Lv, K., Yang, Y., Lu, Z. and Liang, X., Facile synthesis of Co_3O_4 nanoflowers grown on Ni foam with superior electrochemical performance. Electrochimica Acta, 56(14), pp. 4985-4991, 2011. DOI: 10.1016/j.electacta.2011.03.118.

[6] Berenguer, R., Valdés-Solís, T., Fuertes, A.B., Quijada, C. and Morallón, E., Cyanide and phenol oxidation on nanostructured Co_3O_4 electrodes prepared by different methods. Journal of the Electrochemical Society, 155(7), pp. 110-115, 2008. DOI: 10.1149/1.2917210.

[7] Xiao, Y., Hu, C. and Cao, M., High lithium storage capacity and rate capability achieved by mesoporous Co_3O_4 hierarchical nanobundles. Journal of Power Sources, 247, pp. 49-56, 2014. DOI: 10.1016/j.jpowsour.2013.08.069.

[8] Liang, Y., Li, Y. and Wang, H., Co_3O_4 nanocrystals on graphene as a synergistic catalyst for oxygen reduction reaction. Nature Mater, 10, pp. 780-786, 201. DOI:10.1038/nmat3087.

[9] Wang, P., Gu, Y., Miao, L., Zhou, J., Su, H., Wei, A. and Cai, H., Co_3O_4 nanoforest/Ni foam as the interface heating sheet for the efficient solar-driven water evaporation under one sun. Sustainable Materials and Technologies, 20, pp 1-7, 2019. DOI: 10.1016/j.susmat. 2019.e00106.

[10] Lakehal, A., Bedhiaf, B., Bouaza, A., Hadj, B., Ammari, A. and Dalache, C., Structural, optical and electrical properties of Ni-doped Co_3O_4 prepared via Sol-Gel technique. Materials Research, 21(3), pp. 1-7, 2018. DOI: 10.1590/1980-5373-mr-2017-0545.

[11] Mo, S., He, H., Ren, Q., Li, S., Zhang, W., Fu, M. and Ye, D., Macroporous Ni foam-supported Co_3O_4 nanobrush and nanomace hybrid arrays for high-efficiency CO oxidation. Journal of Environmental Sciences, 75, pp. 136-144, 2019. DOI: 10.1016/j.jes.2018.02.026.

[12] Li, S., Wu, K., Li, L., Suo, L. and Zhu, Y., An architecture of dandelion-type Ni- Co_3O_4 microspheres on carbon nanotube films toward an efficient catalyst for oxygen reduction in zinc-air batteries. Applied Surface Science, 481, pp. 40-51, 2019. DOI: 10.1016/j.apsusc.2019.03.053.

[13] Ouyang, K., Guo, G., Liu, Y., Sun, L. and Wei, M., Facile synthesis of heterogeneous Co_3O_4- nanowires/vertical-graphene-nanosheets on Ni foam for high performance supercapacitors. Materials Letters, 251, pp. 176-179, 2019. DOI: 10.1016/j.matlet.2019.05.062.

[14] Ren, Z., Wu, Z., Song, W., Xiao, W., Guo, Y., Ding, J. and Gao, P.X., Low temperature propane oxidation over Co_3O_4 based nano-array catalysts: Ni dopant effect, reaction mechanism and structural stability. Applied Catalysis B: Environmental, 180, pp. 150-160, 2016. DOI: 10.1016/j.apcatb.2015.04.021.

[15] Jin, L., Li, X., Ming, H., Wang, H., Jia, Z., Fu, Y. and Zheng, J., Hydrothermal synthesis of Co_3O_4 with different morphologies towards efficient Li-ion storage. RSC Advances, 4(12), pp. 6083-6089, 2014.

[16] Bahlawane, N., Herve, P., Ngamou, T. and Kohse-höinghaus, K., Functional complex oxides: interplay between the structure, electrical properties and surface reactivity. Society, 516(c), pp. 3282-3282, 2009. DOI: 10.1039/C3RA45904G.

[17] McClure, D.S., The distribution of transition metal cations in spinels. Journal of Physics and Chemistry of Solids, 3(3-4), pp. 311-317, 1957. DOI:10.1016/0022-3697(57)90034-3.

[18] Koneru, A., Non-equilibrium Green' s Function based calculations of spin voltage in cobalt based spinel oxides. PhD. Thesis, Departament of Mechanical and Aerospace Engineering. West Virginia University, Virginia, United States, 2017.

[19] Pan, A., Wang, Y., Xu, W., Nie, Z., Liang, S., Nie, Z. and Zhang, J.G., High-performance anode based on porous Co_3O_4 nanodiscs. Journal of Power Sources, 255, pp. 125-129, 2014. DOI: 10.1016/j.jpowsour.2013.12.131.

[20] Cao, J., Wang, S., Zhang, H. and Zhang, T., Constructing one dimensional Co_3O_4 hierarchical nanofibers as efficient sensing materials for rapid acetone gas detection. Journal of Alloys and Compounds, 799, pp. 513-520, 2019. DOI: 10.1016/j.jallcom.2019.05.356.

[21] Liang, M., Zhao, M., Wang, H., Wang, F. and Song, X., Excellent cycling stabilities of a novel calliandra-like Co_3O_4 acted as anode materials for the lithium-ion battery. Journal of Energy Storage, 17, pp. 311-317, 2018. DOI: 10.1016/j.est.2018.03.017.

[22] Singhal, A., Bisht, A. and Irusta, S., Enhanced oxygen evolution activity of $Co_{3-x}Ni_xO_4$ compared to Co_3O_4 by low Ni doping. Journal of Electroanalytical Chemistry, 823, pp. 482-491, 2018. DOI: 10.1016/j.jelechem.2018.06.051.

[23] Xiao, X., Liu, X., Zhao, H., Chen, D., Liu, F., Xiang, J. and Li, Y., Facile shape control of Co_3O_4 and the effect of the crystal plane on electrochemical performance. Advanced materials, 24(42), pp. 5762-5766, 2012. DOI: 10.1002/adma.201202271.

[24] Deng, S., Liu, X., Chen, N., Deng, D., Xiao, X. and Wang, Y., A highly sensitive VOC gas sensor using p-type mesoporous Co_3O_4 nanosheets prepared by a facile chemical coprecipitation method. Sensors and Actuators B: Chemical, 233, pp. 615-623, 2016. DOI: 10.1016/j.snb.2016.04.138.

[25] Mulinari, T.A., La Porta, F.A., Andrés, J., Cilense, M., Varela, J.A. and Longo, E., Microwave-hydrothermal synthesis of single-crystalline Co 3 O 4 spinel nanocubes. CrystEngComm, 15(37), pp. 7443-7449, 2013. DOI: 10.1039/C3CE41215F.

[26] Li, L., Chu, Y., Liu, Y., Song, J., Wang, D. and Du, X., A facile hydrothermal route to synthesize novel Co_3O_4 nanoplates. Materials Letters, 62(10-11), pp. 1507-1510, 2008. DOI: 10.1016/j.matlet.2007.09.012.

[27] Rajeshkhanna, G. and Ranga Rao, G., Micro and nano-architectures of Co_3O_4 on Ni foam for electro-oxidation of methanol. International Journal of Hydrogen Energy, 43(9), pp. 4706-4715, 2018. DOI: 10.1016/j.ijhydene.2017.10.110.

[28] Rajeshkhanna, G., Umeshbabu, E. and Ranga Rao, G., Charge storage, electrocatalytic and sensing activities of nest-like nanostructured Co_3O_4. Journal of Colloid and Interface Science, 487, pp. 20-30, 2017. DOI: 10.1016/j.jcis.2016.10.011.

[29] Umeshbabu, E., Rajeshkhanna, G., Justin, P. and Rao, G.R., Magnetic, optical and electrocatalytic properties of urchin and sheaf-like $NiCo_2O_4$ nanostructures. Materials Chemistry and Physics, 165, pp. 235-244, 2015. DOI: 10.1016/j.matchemphys.2015.09.023.

[30] Meher, S.K. and Rao, G.R., Effect of microwave on the nanowire morphology, optical, magnetic, and pseudocapacitance behavior of Co_3O_4. Journal of Physical Chemistry C, 115(51), pp. 25543-25556, 2011. DOI:10.1021/jp209165v.

[31] Singhal, A., Bisht, A., Kumar, A. and Sharma, S., One pot, rapid synthesis of Co_3O_4 by solution combustion method and its electrochemical properties in different electrolytes. Journal of Electroanalytical Chemistry, 776, pp. 152-161, 2016. DOI: 10.1016/j.jelechem.2016.07.004.

[32] Itteboina, R. and Sau, T.K., Sol-gel synthesis and characterizations of morphology-controlled Co_3O_4 particles. In: Materials Today: Proceedings, 9, 458-467, 2019. DOI: 10.1016/j.matpr.2019.02.176.

[33] Hu, Z., Oskam, G., Penn, R.L., Pesika, N. and Searson, P.C., The influence of anion on the coarsening kinetics of ZnO nanoparticles. Journal of Physical Chemistry B, 107(14), pp. 3124-3130, 2003. DOI:10.1021/jp020580h.

[34] Lu, B., Cao, D., Wang, P., Wang, G. and Gao, Y., Oxygen evolution reaction on Ni-substituted Co_3O_4 nanowire array electrodes. International Journal of Hydrogen Energy, 36(1), pp. 72-78, 2010. DOI: 10.1016/j.ijhydene.2010.09.056.

[35] Louardi, A., Rmili, A., Ouachtari, F., Bouaoud, A., Elidrissi, B. and Erguig, H., Characterization of cobalt oxide thin films prepared by a facile spray pyrolysis technique using perfume atomizer. Journal of Alloys and Compounds, 509(37), pp. 9183-9189, 2011. DOI: 10.1016/j.jallcom.2011.06.106.

[36] Al-Tuwirqi, R., Al-Ghamdi, A.A., Aal, N.A., Umar, A. and Mahmoud, W.E., Facile synthesis and optical properties of Co_3O_4 nanostructures by the microwave route. Superlattices and Microstructures, 49(4), pp. 416-421, 2011. DOI: 10.1016/j.spmi.2010.12.010.

L.J. Cardenas-Flechas, is BSc. Eng. in Electromechanical Engineering from the Universidad Pedagógica y Tecnológica de Colombia, Duitama, Boyacá in 2014. MSc. in Mechanical Engineering from at the Universidad Nacional de Colombia, Bogotá, Colombia. Currently, she is teaching assistant and PhD candidate in Engineering Materials Science and Technology at the Universidad Nacional Colombia, Bogotá. She has worked on thin films, corrosion resistance and synthesis by physical methods.
ORCID: 0000-0001-6039-3924.

A. Raba, is MsC. in Physics from the Universidad Nacional de Colombia, Bogotá, Colombia. Currently, she is a PhD candidate in Physics at the Universidad Pedagógica y Tecnológica de Colombia and full professor and researcher at the Departamento de Física of the Universidad Francisco de Paula Santander, Colombia.
ORCID: 0000-0001-8147-6323.

M. Rincon-Joya, is full professor at the Departamento de Física of the Universidad Nacional de Colombia, Bogotá Colombia. She conducts research in the general area of development and applications of synthesis by different techniques, analysis of optical properties etc. She received her PhD in 2008 from the Universidade Federal de Sao Carlos, Brasil.
ORCID: 0000-0002-4130-9675